

Passive wire-driven deployable baffle for space debris monitoring

M. Longato⁽¹⁾, M. Honeth^(1,2), G. S. Aglietti^{(1)*}, S. Hosseini⁽³⁾, and C. Bamann⁽³⁾

⁽¹⁾ Space Institute - Te Pūnaha Ātea (TPA-SI), University of Auckland, Auckland, 1010, New Zealand

⁽²⁾ NewSpace Systems, New Zealand

⁽³⁾ Vyoma GmbH, Germany

*Corresponding author, mattia.longato@auckland.ac.nz

ABSTRACT

Telescopic deployable structures optimize launch vehicle options and mission costs by reducing the empty volume occupied by optical payloads. However, these structures require reliable deployment mechanisms. This work develops a passive wire-driven telescopic baffle for larger optical instruments. This study extends the concept to larger optical instruments, requiring baffles that deploy to approximately one meter while stowing at a quarter of that length.

The baffle consists of four concentric CFRP cylinders that slide within each other, actuated by a constant torsion spring mechanism. Three independent deployment wires follow an "S"-shaped path around metallic pins. This synchronized wire tensioning enables uniform deployment, ensuring the final baffle length remains within ± 1 mm of the nominal design. However, variations in sliding dynamics arise from local friction between the moving cylinders and at the various wire bends.

A passive eddy-current damper regulates speed, preventing excessive shock at full deployment. The Hold-Down and Release Mechanism (HDRM) secures the stowed baffle using a tensioned Dyneema wire which is cut by a custom-made thermal knife upon activation. The hold down tension is maintained via parallel linear springs, which compensate for wire relaxation and creep over long-term storage.

Finite Element Analysis (FEA) and motion simulations guide the design choices, ensuring controlled deployment velocity, structural integrity, and compliance with required natural frequencies. Prototyping included an engineering model for initial testing, followed by a qualification model and two flight units. These underwent extensive vibration and thermal-vacuum testing. Deployment reliability was validated using a gravity off-loading system with calibrated constant torque springs, simulating microgravity conditions.

This work advances passive deployable baffle technology for large optical payloads, offering a scalable, mechanically robust solution for future space missions.

1. INTRODUCTION

Optical payloads on satellites, such as star trackers and telescopes, require substantial volume due to optical design constraints. Higher resolution demands larger apertures and longer focal lengths, increasing payload size. However, launch vehicle fairings impose strict volume limitations, making compactness as critical as mass reduction, especially for rideshare missions. While deployable structures are common for solar panels and antennas, deployable optical systems have only been implemented in large-budget projects [9]. Maintaining precise optical alignment adds complexity to deployment mechanisms. However, with the growing use of small satellites, research into compact deployable optical payloads is expanding rapidly. [1].

Deployable optical systems fall into two categories: imagers, where the mechanism directly enhances optical performance by increasing aperture or focal length, and auxiliary structures, such as baffles, that augment optical payloads. High-resolution imagers often use a Cassegrain configuration, where the primary mirror is housed in a barrel, and the secondary mirror is supported at the barrel's end [2]. The barrel size determines the overall instrument dimensions and, consequently, the spacecraft size. In contrast, a deployable optic baffle or barrel can alleviate these spacecraft constraints however, these structures must meet stringent dimensional requirements [3,6]. For deployable barrels, such as the one illustrated in Figure 1B, tolerances are typically in the micrometre and arcsecond range due to the precise positioning required for the secondary mirror, whereas for the baffles such as shown in Figure 1A, the final deployed configuration in space needs to be within the precision of ± 1 millimetre [7,8,10].

Beyond optical elements like mirrors and lenses, many imaging applications require baffles, as illustrated in Figure 1, to block stray light.

The strength of these deployable optic structures consists in moving the "empty" volume that would have been inside the spacecraft towards the outside by saving a considerable amount of space in the satellite [9,10]. On one hand, the use of deployable structures for a baffle could increase its mass, for

example, due to the need to include additional components such as a Hold-Down and Release Mechanism (HDRM) in addition to a motorization system [11,12,13]. A specific trade-off study balancing the ratio of the gained volume inside the satellite against the inevitable fraction of added mass is always required to optimize the overall system.



Figure 1 A) Deployable telescopic baffle demonstration model [4]. B) Breadboard model of a deployable barrel concept [12]

This work focuses on the development of a deployable telescopic baffle characterised by four sliding segments, adaptable to various imaging payloads. This work aims to illustrate the various construction stages from the initial modelling to the final environmental testing. Initially, section 2 illustrates the preliminary numerical models and mechanical design of the various baffle components and FEM. Section 3 shows the assembly stages of the complete baffle, HDRM and deployer. Section 4 shows vibration and thermal testing together with the functional tests with the offloading system to ensure functionality under launch and operational conditions in orbit.

2. GEOMETRY DESIGN

The design of a baffle with internal vanes for an optical system follows an iterative geometric process combined with stray light analysis. This procedure determines the longitudinal position of each vane based on given constraints such as baffle total length (L), stray light exclusion angle, field of view (FoV), and aperture size of the optical element. The primary key design principle consists of avoiding any direct path towards the aperture of the optical element for a ray of light at an angle greater than the specified exclusion angle. Furthermore, any light ray must reflect at least once on any internal baffle wall before reaching the aperture.

As shown in Figure 2 Baffle cross section illustrating the primary design parameters [5] Figure 2, the positions of the internal vanes (V2,V3,V4) of

a single-stage fixed conical baffle are defined by its aperture, half FoV and exclusion angle, which form the main input parameters for the design of the baffle.

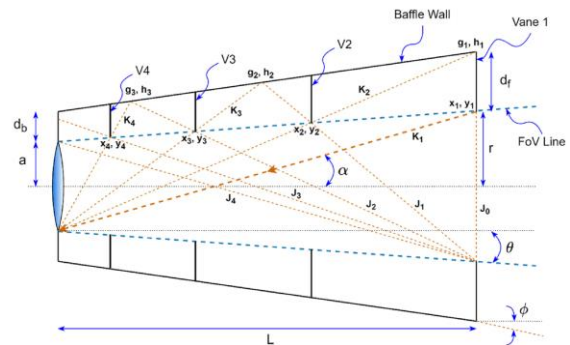


Figure 2 Baffle cross section illustrating the primary design parameters [5]

The front aperture and baffle length depend on the primary optic's half-aperture length (a), exclusion angle (α), and half-FoV (θ). A larger FoV is always preferred because it allows a bigger imaging coverage on the ground. Usually, the available payload volume dictates the optics casing radius (d_b) and the corresponding exit port size (d_f). Usually, lower exclusion angles (α) require longer baffles. Finally, the various vane positions are determined geometrically, ensuring effective light blocking while accommodating payload constraints. In practice, as illustrated in Figure 2, the vane tips should be located at the intersection of the FoV line (dotted blue line), and the rays of light joining the exit port tip and aperture, reflecting via the baffle wall (yellow dotted lines). As a result, this geometrical method must optimize optical performance while considering structural constraints and mass limitations.

Finally, this deployable baffle design optimization process, also needs to consider the additional mass and volume occupied by the complementary passive motorization and the respective Hold Down and Release Mechanism. The motorization includes an aluminum drum actuated by a constant torque spring, storing enough elastic energy to back-wind the three independent Dyneema wires used to deploy the telescopic baffle sections. Additionally, a thicker wire secures the entire baffle, keeping it tightly held during launch. In addition, upon applying a ~ 3 A current to the custom-made thermal knife located in contact with the aforementioned hold down Dyneema wire, the baffle is finally released once in orbit. To conclude, these additional components introduce complexity but are a necessary trade-off to save significant spacecraft volume.

3. DYNAMIC RIGID MODEL

The initial modelling approach for the rigid body motion dynamics of the four moving sections of this

deployable baffle was implemented in MATLAB, using the Simscape Multibody package. The fully deployed baffle shape is shown in Figure 3 while the stowed configuration is shown in Figure 4A. The deployment mechanism, designed to vertically displace each vane consists of a compacted "S" shaped wire path as shown in Figure 4B. The red vertical arrow in the image represents the pulling force required to move the baffle sections. "This force is applied by back-winding three independent Dyneema wires, positioned circumferentially at 120° intervals, using a constant torque spring motorization system.

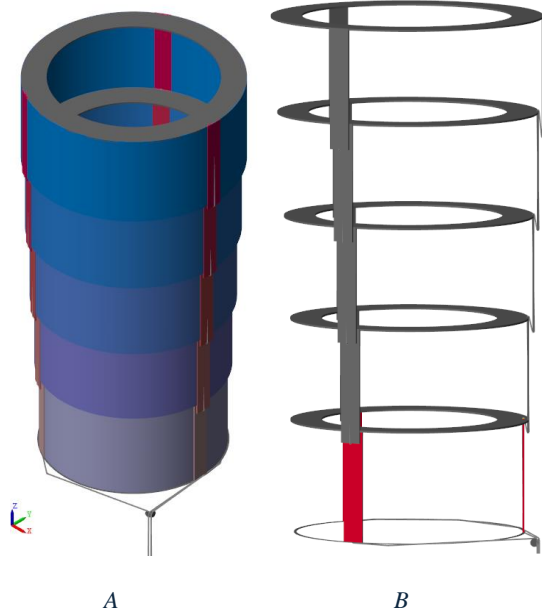


Figure 3 Rigid dynamic baffle model in deployed configuration. A) Deployed vanes. B) Skeleton structure

The five CFRP baffle sections (one stationary and four moving) are composed by an annular vane with three vertical longerons 120° apart and a vertical skirt to block the stray light. All components are modelled as rigid, undeformable bodies with fixed connections with a material density of approximately $\approx 1600 \text{ kg}\cdot\text{m}^{-3}$ in order to match the mass of the real hardware.

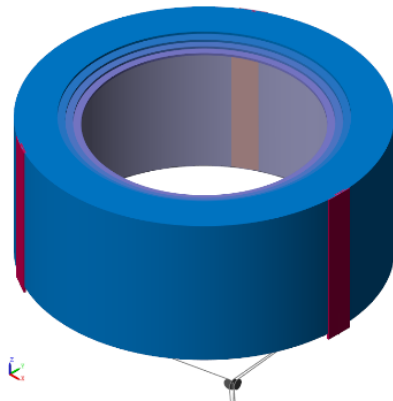


Figure 4 Baffle stowed configuration Simscape model

The "S"-shaped wire path is modelled using the belt-cable circuit blocks running over a concatenated series of pulleys located at each "U" turning point as illustrated in Figure 4B. Furthermore, each pulley is located on a rotational joint which can also include the rotating friction law described in Equation 1.

$$T = \sqrt{2}e(T_{brk} - T_c)e^{-\left(\frac{\omega}{\omega_{St}}\right)^2} \frac{\omega}{\omega_{St}} + T_c \tanh \frac{\omega}{\omega_{Coul}} + f\omega$$

Equation 1 Friction law between rotating bodies

With:

- $\omega_{St} = \omega_{brk}\sqrt{2}$
- $\omega_{Coul} = \omega/10$
- $\omega = \omega_R - \omega_c$

In a similar way, the additional translational friction between each cylindrical sliding vane can be incorporated using the following Equation 2.

$$F = \sqrt{2}e(F_{brk} - F_c)e^{-\left(\frac{v}{v_{St}}\right)^2} \frac{v}{v_{St}} + F_c \tanh \frac{v}{v_{Coul}} + fv$$

Equation 2 Friction law between translating bodies

With:

- $v_{St} = v_{brk}\sqrt{2}$
- $v_{Coul} = v_{brk}/10$
- $v = v_R - v_c$

Both friction laws utilize similar parameters. For rotational friction, Equation 1 involves the torque (T) and rotational velocity (ω) while Equation 2 involves force (F) and linear velocity (v) for the linear friction case. The rotational friction torque (T) in each revolute joint along the "S"-shaped wire path consists of several components: Coulomb friction torque (T_c), breakaway friction torque (T_{brk}), breakaway friction velocity (ω_{brk}), Stribeck velocity threshold (ω_{St}), Coulomb velocity threshold (ω_{Coul}), and the relative angular velocity (ω) between input (ω_R) and output (ω_c) of the pulley joint, multiplied by the viscous friction coefficient (f).

To actuate the baffle's motion, three point-masses at the base are connected to the three independent deployment lines. These masses are tuned to balance the gravitational force with the winding torque provided by the constant torque spring. Additionally, the baffle's moving segments have their mass reduced to 90% of their original weight to simulate the off-loading effect from a second external mechanism.

Consequently, the friction coefficients in the rotational and sliding joints must be iteratively adjusted to simulate the baffle's full opening dynamics within the desired deployment time. Figure 5 and Figure 6 show the linear displacement and sliding velocity of the top section of the last moving vane.

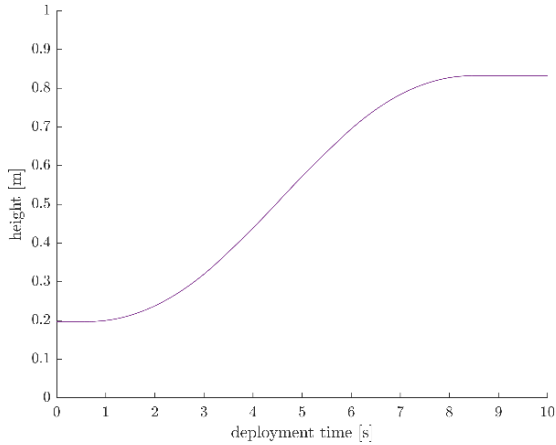


Figure 5 Deployment baffle displacement of the last vane

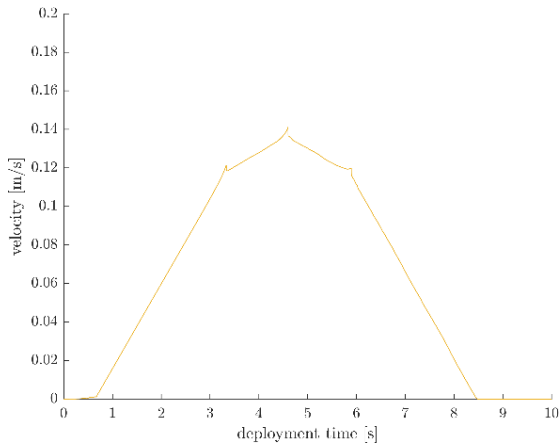


Figure 6 Deployment baffle velocity of the last vane

The simulation shows how the baffle gradually deploys to a final height of approximately $\approx 0.880 \text{ mm}$, with a peak velocity of around $\approx 0.14 \text{ m/s}$.

To conclude, depending on the various friction coefficients, this model is able to reliably represent the complex dynamics that occur in space (without gravity) and during the various functional deployment tests carried out on ground.

4. DEPLOYMENT MECHANISM & THERMAL KNIFE SYSTEM

Regarding the deployable baffle mechanism, a simplified schematic representation is shown in Figure 7A. This mechanism utilises two parallel-mounted spools: a storage spool and a drive spool. Initially, the constant torque spring shown with the red line in Figure 7 is wound onto the drive spool, storing enough energy to move the four baffle sections by pulling the deployment lines. A gear train, mounted on one side of the drive spool, connects to a custom-made eddy-current damper. This device is designed to limit the final baffle end-of-run shock during the deployment. This device is able to produce on one hand a considerable amount of damping torque proportional to the sliding speed of the baffle's vanes, whereas, on the other hand, it ensures a frictionless rotating condition of the drive

spool when deployment starts.

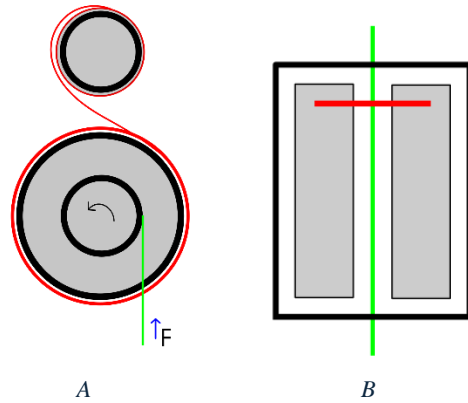


Figure 7 A) Passive spring driven deployer mechanism.
B) Custom made burn wire actuator

The baffle opening command occurs when a current is applied to the custom-made burn wire actuator, schematised in Figure 7B. The concept of this thermal knife consists of an incandescent Kanthal wire shown in red which is positioned perpendicular and pressed against the additional Dyneema wire shown in green adopted for the Hold-Down and Release Mechanism (HDRM). When the burn wire system is actuated, the hold-down Dyneema wire is thermally cut, allowing the constant torque spring to unwind onto the storage spool. This simultaneously pulls the three deployment lines onto the drive shaft, extending the baffle segments.

5. FINITE ELEMENT MODEL

Similar to the dynamic model illustrated in Section 3, the structural frequency response and deformation of the baffle assembly has also been investigated with various finite element analyses. Key parameters, such as the thickness and lay-up configuration of the CFRP in the cylindrical shells and annular vanes, were iteratively adjusted to meet design requirements. Standard modal analyses are performed on the stowed and deployed baffle configuration illustrated in Figure 8 and in Figure 11 to verify compliance with natural frequency requirements. The required minimum natural frequency is 40 Hz in the stowed configuration and 6 Hz in the deployed configuration.

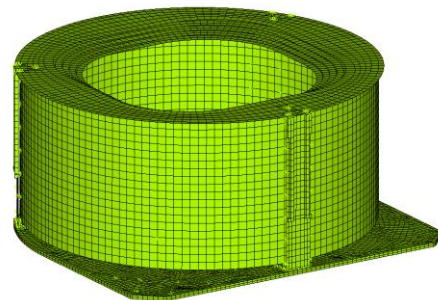


Figure 8 Baffle finite element model

Furthermore, the capability to withstand the launch QSL and random vibration environment is assessed by performing additional static and frequency response analysis. Ultimately, the structural response initially predicted with these models is later verified with the various test campaigns described in the next section.

Additionally, the FEM is used to analyse the stiffness properties of the connections between baffle components. Specifically, the potential criticality of the “parallelogramming” effect illustrated in Figure 9 is investigated to ensure a sufficient shear stiffness between the vanes in order to limit the relative displacements during the application of lateral vibrations. This is a crucial feature to ensure that the requirement of the 40 Hz on the lowest natural frequency is met in the stowed configuration during launch.

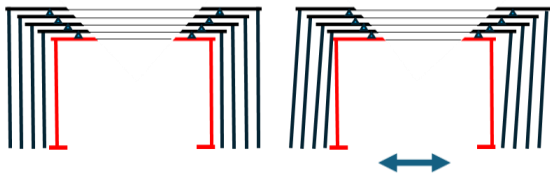


Figure 9 Schematic cross section of the baffle illustrating “parallelogramming” under lateral vibration

Finally, an additional series of coupled load analyses of the baffle are performed by incorporating the main structure of the spacecraft in the finite element model as shown in Figure 10 and in Figure 11. These simulations are essential to understand and predict the dynamic interactions and load paths between the satellite and the payload.

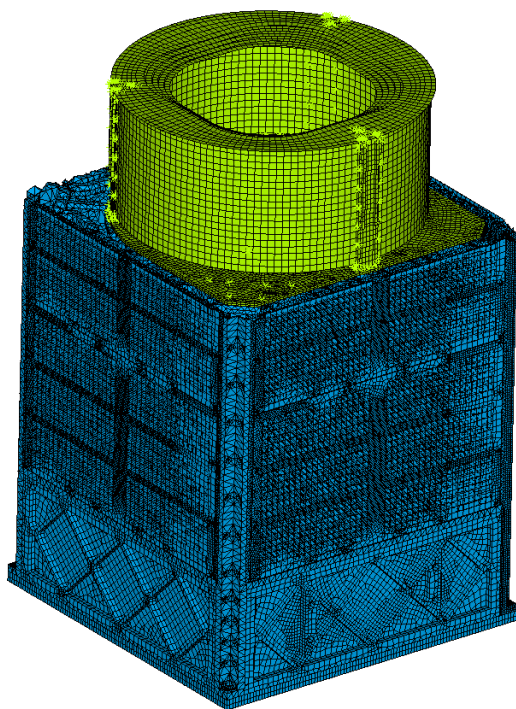


Figure 10 Main satellite structure and baffle finite element model

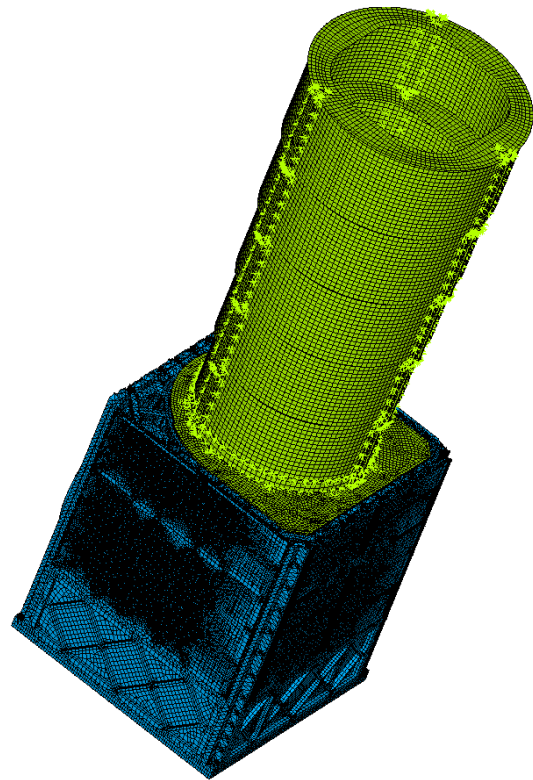


Figure 11 Satellite and baffle in the deployed configuration for in orbit coupled structural analysis

As a result, various structural response comparisons are performed between the standalone baffle model and the model coupled with the satellite. Ultimately, these predictions must be validated with the following environmental tests campaigns.

6. BAFFLE ASSEMBLY

As a result of the previous analyses, the optimal shape of the baffle components was determined, allowing them to be finalized and ordered for manufacturing.



Figure 12 Baffle vane and longerons

Figure 12, illustrates three of the five annular vanes of the baffle and the five triplets of longerons. On the other hand, Figure 13A shows a circular CFRP skirts that are manually curved into a cylindrical shape before being glued on the respective vane shown in Figure 12.

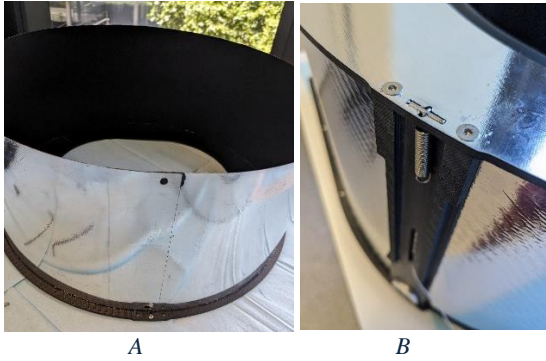


Figure 13 A) Circular skirt and vane integration. B) Vane to longeron bolted connection

Furthermore, each group of three longerons illustrated in Figure 12 must be vertically screwed into the corresponding vane as depicted in Figure 13 B. The vertical height of each group of three longerons is a crucial dimension since they determine the precise vertical location of the vanes. This is essential to ensure a proper engagement between the five moving vanes in the baffle stowed configuration and thus minimize the potential structural “parallelogramming” as depicted in Figure 9. This assembly process is illustrated in Figure 14, where every section is pre-assembled with 1 kg of compressing preload to verify the proper seating of the longeron foot with the CFRP base of the baffle.

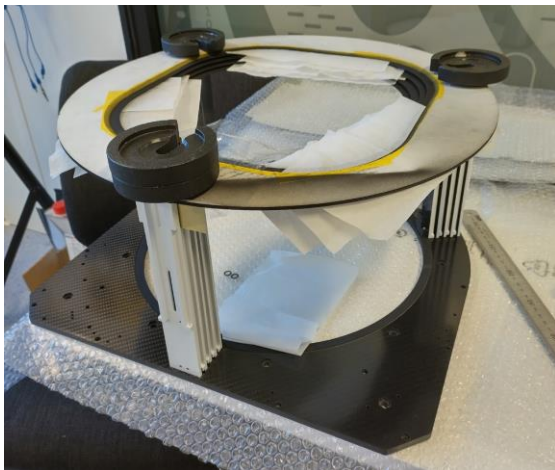


Figure 14 Baffle skeleton assembly stage

Once the individual cylinders are assembled, the three independent deployment Dyneema lines introduced in Section 2 are routed between the skirts through dedicated guide channels along the longerons and inside the base. As a result, the final deployed baffle structure is illustrated in Figure 15. The outer surface of each skirt and the top of the last moving vane are coated with a reflective layer that is applied during the lamination process ensuring uniform and durable coverage. Similarly, the inner black coating requires a manual spray-painting process to guarantee an effective suppression of the

unwanted light, which is critical to the baffle’s performance.



Figure 15 Deployed configuration of the baffle flight unit

7. TESTING

Various test campaigns are conducted on this deployable baffle structure. First, several functional deployment experiments are performed to characterise the actual sliding friction between the cylindrical sections.



Figure 16 Functional deployment baffle test with off-loading passive mechanism

As shown in Figure 16, every baffle moving segment is independently supported vertically by the custom-made offloading device. Depending on the percentage of offloaded baffle mass, various dynamic scenarios can be assessed, ranging from excessively rapid deployment to deployment failure due to self-weight. These functional tests also help refine the friction parameters in the initial dynamic

models discussed in Section 2.

On the other hand, the environmental qualification tests are conducted to experimentally verify the structural design requirements as outlined in Section 4 and cross-validate the predictions of the finite element models from Section 5. The various vibration tests performed include:

- Natural frequency higher than 40 Hz when in stowed configuration i.e. launch configuration.
- Natural frequency higher than 6 Hz when deployed i.e. in orbit operations (cantilevered configuration, rigidly constrained at the mounting points).
- Capability to withstand 4 g sinusoidal excitation (from 5 Hz to 100 Hz, with a sweep rate of 2 oct/min)
- Capability to withstand a random vibration environment as specified in GEVS [8] (14.1 g_{RMS} for Qual and 10.0 g_{RMS} for acceptance)

For example, the lateral stowed configuration vibration test is shown in Figure 17 where various accelerometers are placed on the top of the last vane to verify the lowest lateral resonant frequency of the structure. In this case, thanks to the correct positioning of the vane-to-vane contact points and the closing pressure applied with the Hold-Down system, the four sliding baffle segments are firmly secured and locked into the base plate. Consequently, as indicated in Figure 18, the first natural lateral frequency was found approximately 80 Hz with a notable damped shape due to the unavoidable contact friction acting between the various telescopic cylinders.

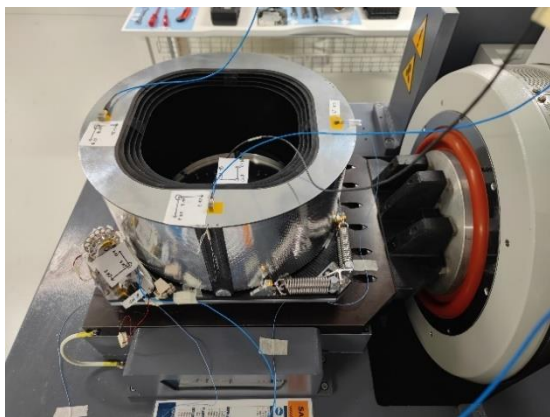


Figure 17 Lateral vibration test campaign along Y-axis in the stowed configuration

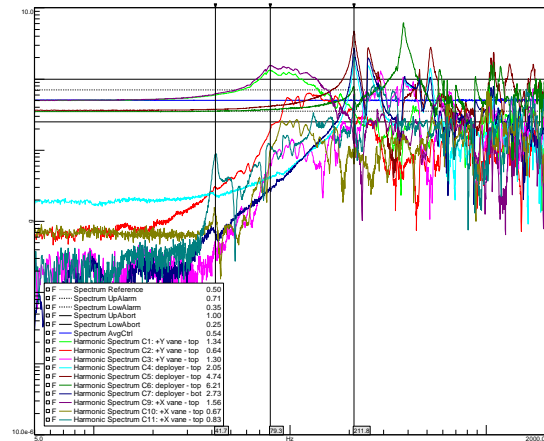


Figure 18 Lateral baffle response curves along the Y-axis with sine sweep input at 0.5g.

Similarly, the vibration test in the vertical stowed configuration is illustrated in Figure 19. In this case, the resonant frequency was approximately 230 Hz which is much higher than the required 40 Hz for the launch configuration.

Finally, a thermal-vacuum testing, demonstrated the capability of the baffle components and the Dyneema wire used for the HDRM and deployment to survive in both hot and cold environments reaching temperatures from -35°C to +70°C. After this sequence of tests, one additional deployment test was necessary to assess and verify the correct functionality of the mechanics. This final successful deployment demonstrated that this baffle model is able to withstand and meet all the system level requirements imposed with additional margin.

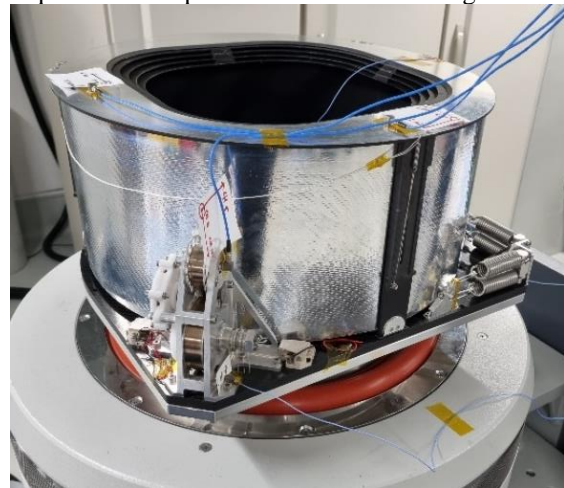


Figure 19 Vertical vibration test campaign along Z-axis in the stowed configuration

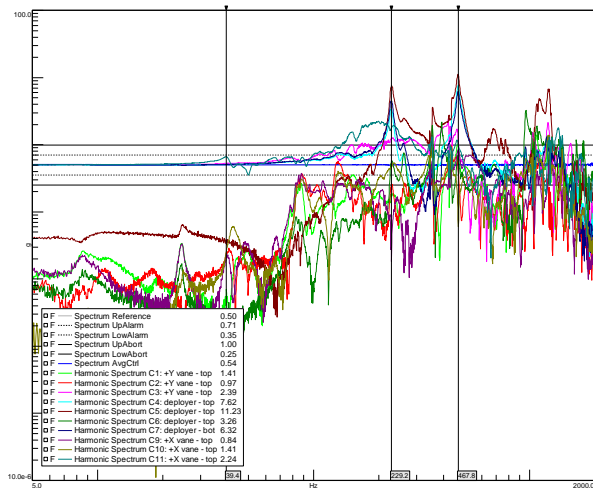


Figure 20 Vertical baffle response curves along the Z-axis with sine sweep input at 0.5 g

8. CONCLUSIONS

This article presents the development of a deployable baffle mechanism for a 100 kg-class satellite. Initially various mathematical and FEM models are developed to investigate the dynamics of this telescopic structure and guide the design in order to meet the given system level requirements. A considerable challenge was the high non-linearity of the mechanism because this passive deployment structure involves a considerable number of contact features and sliding/rolling components. For this reason, various functional tests were performed to verify the correctness of the deployment dynamics under different boundary conditions. Similarly, the manufacturing and the assembly process posed various challenges such as the managing of the friction of the deployment lines, the alignment of the sliding baffle sections, the bonding of the cylindrical skirts within the drawing tolerances. Lastly, extensive testing of the HDRM and deployment mechanism ensured the reliability of the custom-made design. Lessons learned from this process offer valuable insights for future space-based deployable structures.

9. REFERENCES

1. Heinisch, R.P., Jolliffe, C.L., (1971). *Light baffle attenuation measurements in the visible*. Appl. Opt. 10, 2016–2020. <https://doi.org/10.1364/ao.10.002016>.
2. Haghshenas, J. and Johari E. (2014). A theoretical method for vanes profile design in star sensor baffle. In *Earth Observing Missions and Sensors: Development, Implementation, and Characterization III* (Vol. 9264, No. 74, p. 92641R). doi: 10.1117/12.2069467.
3. Arnoux, J.-J.P. (1996). *Star sensor baffle optimization: some helpful practical design rules*. Opt. Syst. Contam. V, Stray Light Syst. Optim. 2864, 333–338. <https://doi.org/10.1117/12.258324>.
4. Yalagach, A., Honeth, M., Gandhi, R., Aglietti, G.S., Ingram, C., Saxena, A. (2024). *Development of a deployable mechanism for a conical optical baffle for a small satellite*. Adv. Space Res. 73(1), 870-884. <https://doi.org/10.1016/j.asr.2023.11.010>.
5. Yalagach, A., Aglietti, G.S., Honeth, M., et al. (2021). *Deployable barrel for a cubesat's optical payload*. AIAA (pp. 1-10). <https://doi.org/10.2514/6.2021-1791>.
6. Gooding, D., Richardson, G., Haslehurst, A., et al. (2018). *A novel deployable telescope to facilitate a low-cost & 1m gsd video rapid revisit small satellite constellation*. In Proc. SPIE 11180, 1118009. <https://doi.org/10.1117/12.2535928>.
7. Tae-Yong, P., Bong-Geon, C., & Hyun-Ung, O. (2019). *Development of 6U cubesat's deployable solar panel with burn wire triggering holding and release mechanism*. Int. J. Aerospace Eng. 2019, Article ID 7346436. <https://doi.org/10.1155/2019/7346436>
8. NASA (2013). *General Environmental Verification Standard (GEVS) for GSFC Flight Programs and Projects*. Goddard Space Flight Center Standards, Vol. 7000. NASA, Greenbelt, MD. Available from: <https://standards.nasa.gov/standard/gsfsc/gsfsc-std-7000>.
9. Gardner, J.P., Mather, J.C., Clampin, M., et al., 2006. *The james webb space telescope*. Space Sci. Rev. 123, 485–606. <https://doi.org/10.1007/s11214-006-8315-7>.
10. Edeson, R., Aglietti, G.S., Tatnall, A.R., 2010. *Conventional stable structures for space optics: The state of the art*. Acta Astronautica. 66, 13–32. <https://doi.org/10.1016/j.actaastro.2009.06.015>.
11. Honeth, M., Yalagach, A., Aglietti, G.S., 2022. *Wire driven mechanisms for deployable components for optical payloads*. volume SSC22-WKVI-06, 1–9.
12. Shore, J., Blows, R., Viquerat, A. et al., 2019. *A new generation of deployable optics for earth observation using small satellites*. European Space Mechanisms and Tribology Symposium 2019, Munich, Germany.
13. Choi, J., Lee, D., Hwang, K., et al., 2019. *Design, fabrication, and evaluation of a passive deployment mechanism for deployable space telescope*. Adv. Mech. Eng. 11, 1–14. <https://doi.org/10.1177/1687814019852258>.